Received: 30 September 2023 | Revised: 7 November 2023 | Accepted: 11 November 2023

DOI: 10.1111/php.13890

RESEARCH ARTICLE

Photocatalytic fixation and oxygenation of NAD^+/$NADP^+$ and sulfides using solar light: Exploring mechanistic investigations and their impact on synthetic applications

Ravindra K. Shukla[1] | **Rajesh K. Yadav**[1] | **Vittal L. Gole**[2] | **Satyam Singh**[1] | **Navneet Kumar Gupta**[3] | **Jin-Ook Baeg**[4]

[1]Department of Chemistry and Environmental Science, Madan Mohan Malaviya University of Technology, Gorakhpur, India

[2]Department of Chemical Engineering, Madan Mohan Malaviya University of Technology, Gorakhpur, India

[3]Centre for Sustainable Technologies, Indian Institute of Science, Bengaluru, India

[4]Artificial Photosynthesis Research Group, Korea Research Institute of Chemical Technology, Daejeon, Korea

Correspondence

Rajesh K. Yadav, Department of Chemistry and Environmental Science, Madan Mohan Malaviya University of Technology, Gorakhpur, UP 273010, India.
Email: rajeshkr_yadav2003@yahoo.co.in

Jin-Ook Baeg, Artificial Photosynthesis Research Group, Korea Research Institute of Chemical Technology, Yuseong-gu, Daejeon 34114, Korea.
Email: jobaeg@krict.re.kr

Abstract

Sulfur-doped Eosin-B (SDE-B) photocatalysts were synthesized for the first time utilizing sublimed sulfur (S_8) as a dopant in an in situ thermal copolymerization technique. Sulfur doping not only increased Eosin-B (E-B) absorption range for solar radiation but also improved fixation and oxygenation capabilities. The doped sulfur bridges the S-S bond by substituting for the edge bromine of the E-B bond. The improved photocatalytic activity of SDE-B in the fixation and oxygenation of NAD^+/$NADP^+$ and sulfides using solar light is attributed to the photo-induced hole of SDE-B's high fixation and oxygenation capacity, as well as an efficient suppression of electron and hole recombination. The powerful light-harvesting bridge system created using SDE-B as a photocatalyst works extremely well, resulting in high NADH/NADPH regeneration (79.58/76.36%) and good sulfoxide yields (98.9%) under solar light. This study focuses on the creation and implementation of a sulfur-doped photocatalyst for direct fine chemical regeneration and organic transformation.

KEYWORDS

1,4-NADH/NADPH regeneration, oxygenation reaction, SDE-B, solar light

INTRODUCTION

Pharmaceutically usable solar fine chemical production, such as NADH regeneration and oxygenation of sulfide under solar light, is very important for the scientific society.[1,2] In this context, oxidation (sulfide) and reduction (NAD^+) are one of the most captivating transformations of organic compounds[3] and selective regeneration of NADH and have been expansively studied in the previous periods.[4–8] Conventionally, toxic/hazardous reducing and nonreducing agents, such as very toxic expensive metal oxides, methyl viologen, and organic peroxides in stoichiometric quantities, were generally utilized for these chemical conversions in terms of oxidation and reduction.[9–12] Therefore, a photocatalytic, cost-effective, and environmentally friendly reduction and oxidation method is constantly needed through the utilization of solar light as a green[13] and traceless reagent. In this context, photochemistry is a significant and potent synthetic approach that can facilitate numerous functional group transformations[14–22] and regeneration of NADH. In recent years, solar light-driven photocatalysis has emerged as a key area of synthetic methods[23–27] due to the fact that it provides environmentally friendly alternatives to a number of traditional synthetic processes.

Consequently, it has been determined that photocatalysis complies with the ideas of the many methods of Green Chemistry[27] for oxygenation reactions and reduction in NAD^+. The incorporation of oxygen into a substrate using photosensitized oxygenation has been acknowledged as a contemporary technique. The molecular oxygen activation by a sensitizer's excited state is the foundation of photo-oxygenation. Either singlet oxygen or the electron transfer (ET) process can cause it to happen.[28] However, the use of expensive and dangerous metals severely restricts its practical application. A nonmetal photocatalytic photoreactor offers an environmentally favorable alternative synthetic method for selective oxidation and reduction under mild conditions due to its cheaper cost and widespread availability.[29,30] Since many sulfoxides and NADH are biologically active chemicals and production of energy through redox reactions is frequently utilized in pharmaceutical industries,[31,32] chemo-selective transformation of sulfides to sulfoxides and conversion of NAD^+ to NADH is of great interest (Scheme 1). Sulfoxidation is also advantageous for the synthesis of organic materials, the desulfurization of fossil fuels, the treatment of industrial wastes, and the destruction of chemical weapons.[33–39] However, NADH is also a significant industrial chemicals, which can be utilized in various medicines.[40–42] There is a need for environmentally friendly and gentle sulfide oxidation and NAD^+ reduction processes that produce sulfoxides chemo-selectively without over-oxidation to sulfones and regenerate NADH. As per our group concern, the main problems of using peracids/methyl viologen in industrial processes are the over-oxidation/reduction to sulfones/NAD^+ and the safety and system corrosion concerns with handling peracids.[32] The photooxidation/reduction of sulfides/NAD^+ was studied using a variety of expensive sensitizers, including organic molecules, inorganic materials,[43–49] and metal complexes.[50–53] Additionally, certain photocatalysts are unstable, which makes it challenging to use them in commercial processes. These factors make a more durable organic photocatalyst that can oxidize and reduce both a wide range of sulfides and NAD^+ particularly desirable. Due to their tunable emission and absorption characteristics, EOSIN-B (E-B) have become a group of fluorescent organic light-harvesting dye molecules, similar to the light-harvesting compounds. Due to their tunable backbone, many researchers are it utilizing in various research fields such as organic photovoltaics, sensor, organic field-effect transistors, supramolecular assemblies, and organic field-effect transistors. There

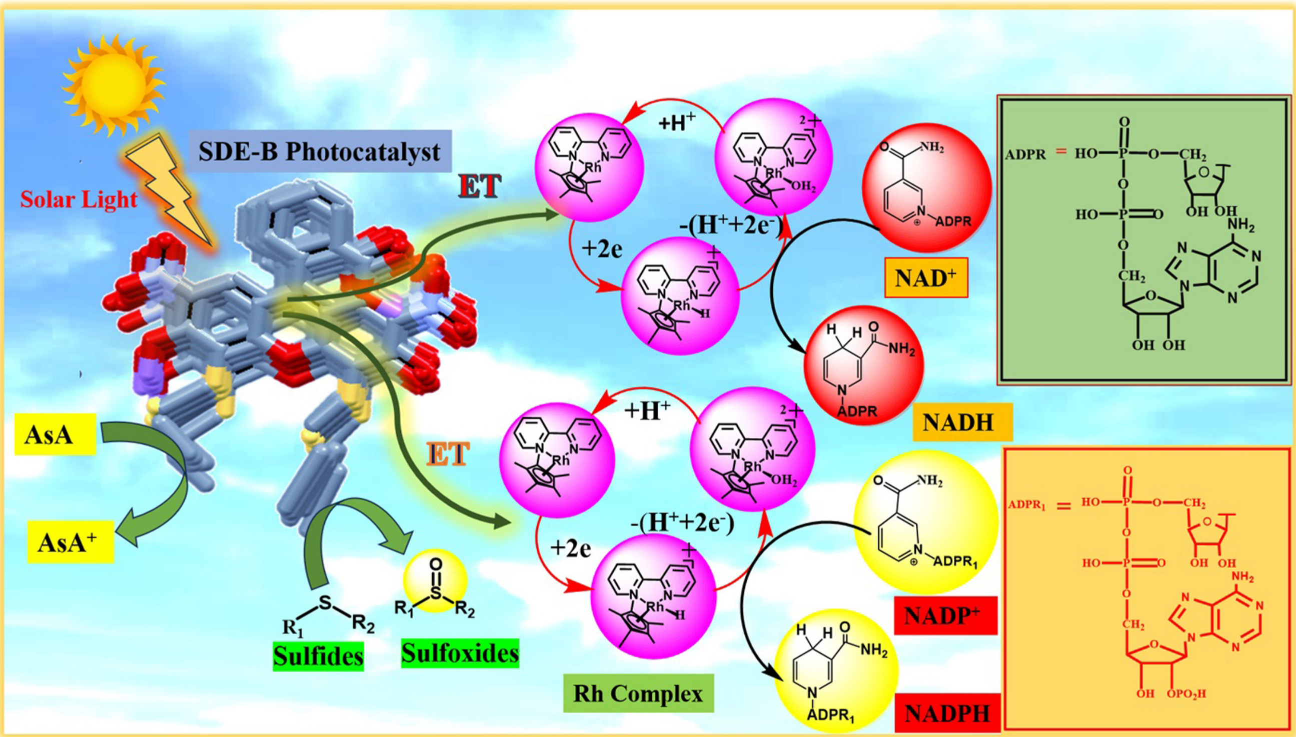

SCHEME 1 Pictorial illustration of an artificial photosynthetic system mimicking the natural photosynthetic system for fixation of NAD^+/$NADP^+$ into NADH/NADPH along with oxygenation of sulfides via newly designed SDE-B photocatalyst under solar light.

is limited research on the application of SDE-B as solar light-driven photocatalysts for synthetic transformations and NADH/NADPH regeneration,[54] particularly for selective aerobic oxidation, despite these outstanding features of SDE-B such as photosensitizer. Here, we describe a solar light-mediated photo-oxygenation of sulfides to sulfoxides and selective regeneration of cofactor of 1,4-NADH/NADPH using SDE-B as the photocatalyst (Scheme 1).

MATERIALS AND METHODS

Materials

Eosin-B, sublimed sulfur (S_8), chloroform ($CHCl_3$), dimethylformamide (DMF), triethylamine (TEA), isopropyl alcohol (IPA), ethanol (EtOH), 4-(methylthio) benzaldehyde, 4 chlorobenzene thiol, methyl-p-tolyl sulfide, 2-aminobenzenethiol, 1,3,5-triazine-2,4,6- trithiol, silica gel, hexane, ethyl acetate, ascorbic acid, NAD^+, $NADP^+$ pentamethylcyclopentadienyl rhodium (III) dichloride dimer, and 2, 2′bipyridy were used as such and purchased from Sigma-Aldrich.

Synthesis of sulfur-doped Eosin-B (SDE-B) photocatalysts

The 1.0 g Eosin-B and 3.0 g sublimed sulfur (S_8) were homogeneously mixed by the mortar pastel method, and after that mixed material was collected in the crucible. The crucible was shifted in a muffle furnace for 2 h (ramping rate: 1°C min^{-1}) at 160°C. After cooling, the crucible was removed from the same. After that, the gray color product was obtained (1.98 g), which is purified by water and acetone (Scheme 2).

General procedure for photocatalytic oxygenation of sulfides

In a dried vial tube equipped with a small magnetic stir, the initial reactant (sulfides) (0.2 mmol) and SDE-B photocatalyst (5 mg) were dissolved in 4.0 mL of isopropyl alcohol (IPA) under the aerobic situation. After that, the solution was irradiated under solar light for few hours at room temperature in aerobic conditions. The reaction completion condition was examined by the standard thin-layer chromatography (TLC). After the completion of the running reaction, the reaction mixture was concentrated under reduced pressure. The as-obtained final product was refined by using column chromatography based on silica gel (hexane/ethyl acetate: 10:1) to afford the corresponding sulfoxide.[55]

Photocatalytic fixation of the NAD^+/$NADP^+$ by newly designed SDE-B photocatalyst

The photocatalytic fixation of the NAD^+/$NADP^+$ from the SDE-B photocatalyst photocatalysts quickly transfers the excited electrons for NADH/NADPH coenzyme regeneration via ORC. The cofactor regeneration of 1,4-NADH/NADPH was 79.58% and 76.36% in 2 h shown in Figure 3. The photocatalytic fixation of NAD^+/$NADP^+$ was performed under solar radiation at room temperature. The reaction was carried in a dried vial tube equipped with a small magnetic stir by mixing the NAD^+/$NADP^+$ (1.24 μmol), ORC complex (0.62 μmol), ascorbic acid (AsA) (0.1 mmol) as a sacrificial agent and SDE-B photocatalyst (5 mg) mixed in 3100 μL neutral sodium phosphate buffer solution (100 mM). The photocatalytic output of NADH/NADPH regeneration via SDE-B photocatalysts were monitored by the reported method.[56,57]

RESULTS AND DISCUSSION

Strategy of the artificial photosynthetic photoreactor for mimicking the natural photosynthetic mechanism

In Z-scheme of the natural photosynthetic system contained two types of photosystem (PS) segments, that is, PS-700(I) and PS-680(II) as shown in Scheme 3. Chlorophyll containing PS-680(II) serves as the reaction center for the absorption of solar light. The capture of solar light in the PS-680(II) produces photo-excited electrons, due to which the electron-mediating components, such as the cytochrome complex, move to the plastocyanin (PC) complex. The movement of photo-excited electron via ferredoxin $NADP^+$ oxidoreductase into NADPH after the PC complex reduces the photo-oxidized PS-700(I). Therefore, natural photosynthetic PS-700(I) and PS-680(II) systems play an important role in the making of valuable NADH/NADPH coenzymes under solar light radiation.[58–62] On the basis of natural photosynthesis, we design highly efficient SDE-B artificial photosynthetic photoreactor for NADH/NADPH regeneration. The reaction mechanism for the regeneration of NADH/NADPH coenzymes via a photocatalytic

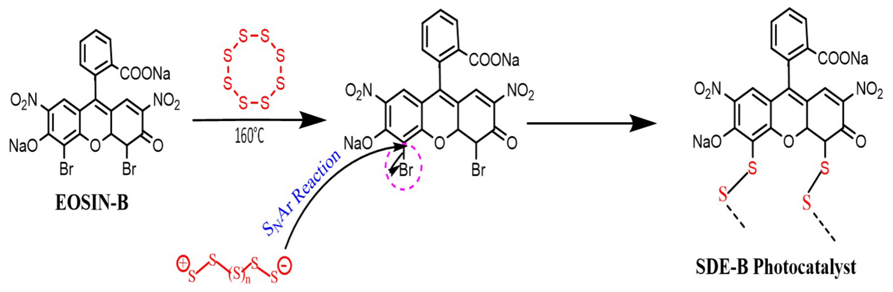

SCHEME 2 Synthesis of sulfur-doped Eosin-B (SDE-B) photocatalysts utilizing sublimed sulfur (S_8) as a dopant in an in situ thermal copolymerization technique.

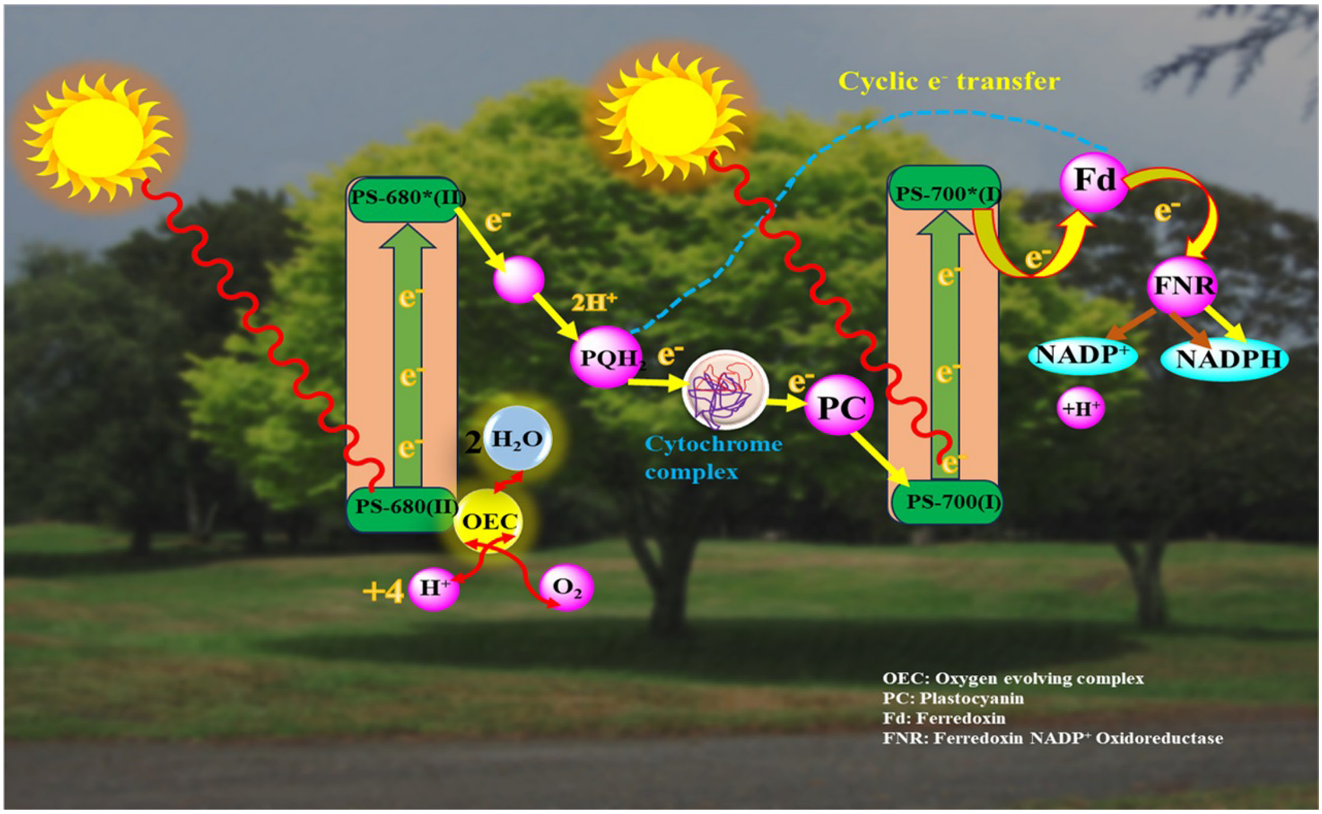

SCHEME 3 Pictorial illustration of Z-scheme of the natural photosynthetic system.

route under solar light is shown in Scheme 1. As per Scheme 1, the transfer of electrons between SDE-B photocatalysts and ORC complex is more similar to the electron transfer routes between PS-700(I) and PS-680(II) detected in the natural photosynthesis.[58–62] The highly light-harvesting bridge system captures solar light irradiation-generated photo-excited electrons transfer from SDE-B photocatalyst to ORC complex that easily takes electron and gets reduced. ORC takes proton from aqueous buffer medium and the electrons transferred to oxidized form NAD+/NADP+ and reduces to fine chemicals in the form of NADH/NADPH. In this mechanism, ORC works as electron and proton transfer mediator between SDE-B photocatalysts and NAD^+/$NADP^+$. Instead, the newly designed SDE-B photocatalyst has also an additional capability for oxygenation reaction under solar light.

Characterization of newly designed SDE-B photocatalyst

Figure 1A's representation of the UV–visible absorption spectra of SDE-B photocatalyst for solid-state powders shows that SDE-B photocatalyst exhibits wide solar light absorption in 475–500 nm range, which is comparable to that of the Eosin-B (E-B) monomer (Figure S1) and suggests that the SDE-B photocatalyst networks have the

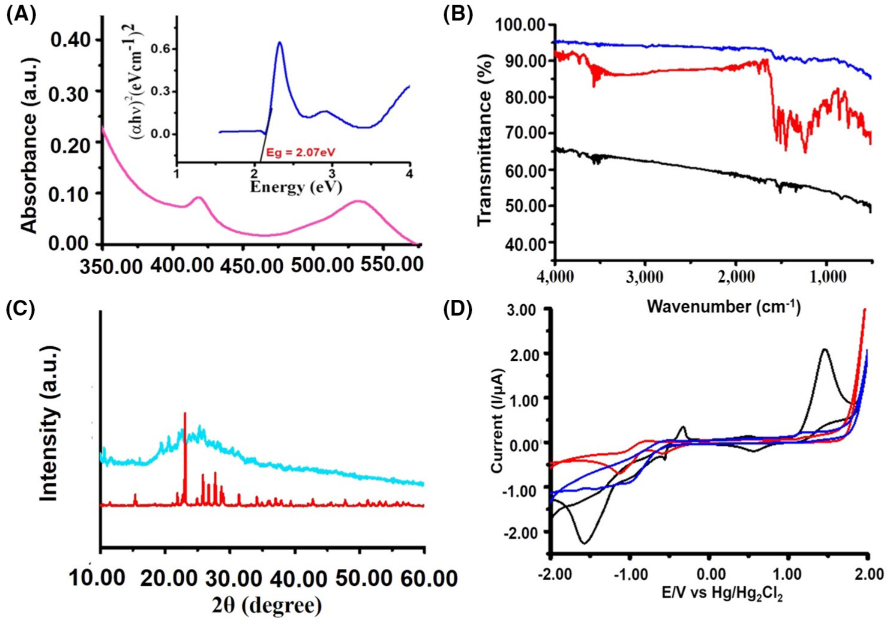

FIGURE 1 (A) UV–visible absorption spectra of SDE-B photocatalyst along with tau plot for calculation of energy band gap (2.07 eV); (B) FTIR spectra of S_8 (black), E-B (red) monomers and SDE-B (blue) photocatalyst; (C) XRD pattern of E-B (indigo) and SDE-B photocatalyst (red); and (D) cyclic voltammograms of E-B (black), S_8 (red), and mixture of SDE-B + ROC + NAD^+ for mechanistic studies. The potential was scanned at 100 mV s^{-1} using glassy carbon as working electrode, Hg/$HgCl_2$ as a reference electrode, and platinum as a counter electrode in neutral sodium phosphate buffer (100 mM).

ability to absorb light over a broad range or area of the solar spectrum. Therefore, the newly designed SDE-B photocatalyst has superior photocatalytic activity than the E-B monomer. The absence of the bromine bending peak of the C-Br group at about 772 cm^{-1} in the FT-IR spectra of the SDE-B photocatalyst recommended that most of the C-Br group in the starting substrate have been utilized to form -C-S- groups in the newly designed networks. Furthermore, a comparison of the FTIR spectra of SDE-B and E-B photocatalysts revealed unique characteristics. The production of S-S bonds was indicated by the observation of a strong and bright band at about 599 cm^{-1},[63] which was noticeably lacking in E-B (Figure 1B). Additionally, a new band at roughly 670 cm^{-1} was found, which corresponds to the creation of a C-S bond (Figure 1B).[64] Due to the presence of the carboxylate group, the bond associated with the terminal thiol was not readily evident in the FTIR spectra (Figure 1B).The high degree of spectral of SDE-B photocatalyst demonstrates the structural phenomenon of this material (Figure 1C). XRD patterns of E-B and SDE-B photocatalysts are exhibited in Figure 1C. Power X-ray diffraction measurements indicate that the SDE-B photocatalyst network is amorphous in nature as per reported networks[65] Figure 1C demonstrates the X-ray diffraction for pure E-B dye monomer and SDE-B photocatalysts, respectively. It was noted that various strong peaks appear on the pattern E-B compared with SDE-B photocatalysts. Additionally, the photocatalyst was discovered to be amorphous and to have a broad peak in the range of 16° to 35° in the PXRD investigation (Figure 1C). In contrast to amorphous chemicals, which often show weak intensity peaks or relatively flat XRD patterns,[66] crystalline substances typically show prominent and sharp peaks in XRD graphs.[67] Long-range atomic disorder in this kind of amorphous material offers them unique mechanical, optical, electrical, and magnetic properties. Charge carriers are trapped by the long-range disorder, making it easier for them to separate, encouraging effective redox reactions.

The SEM image of SDE-B photocatalysts displayed different morphologies than E-B monomer (Figure S3), but rough surfaces and the particles were on the order of micrometers in size (Figure 2C). SEM was used to analyze the surface morphology of the photocatalyst in order to better understand its involvement in photocatalysis. The existence of a dumbbell shape may be shown with localized aggregation[64] in Figure 2C. The elemental composition of the photocatalyst was also evaluated using the SEM-EDS method (Figure S4), which corroborated the presence of carbon, oxygen, sodium, and sulfur and demonstrated that SDE-B photocatalysts form as a result of the absence of bromine. A potent imaging method was used to view the microstructure of materials at a very high-resolution TEM.It appears that TEM was used to evaluate a sample, and the outcomes are shown in Figure 2B. Some details concerning the morphology of the substance seen in Figure 2B are given

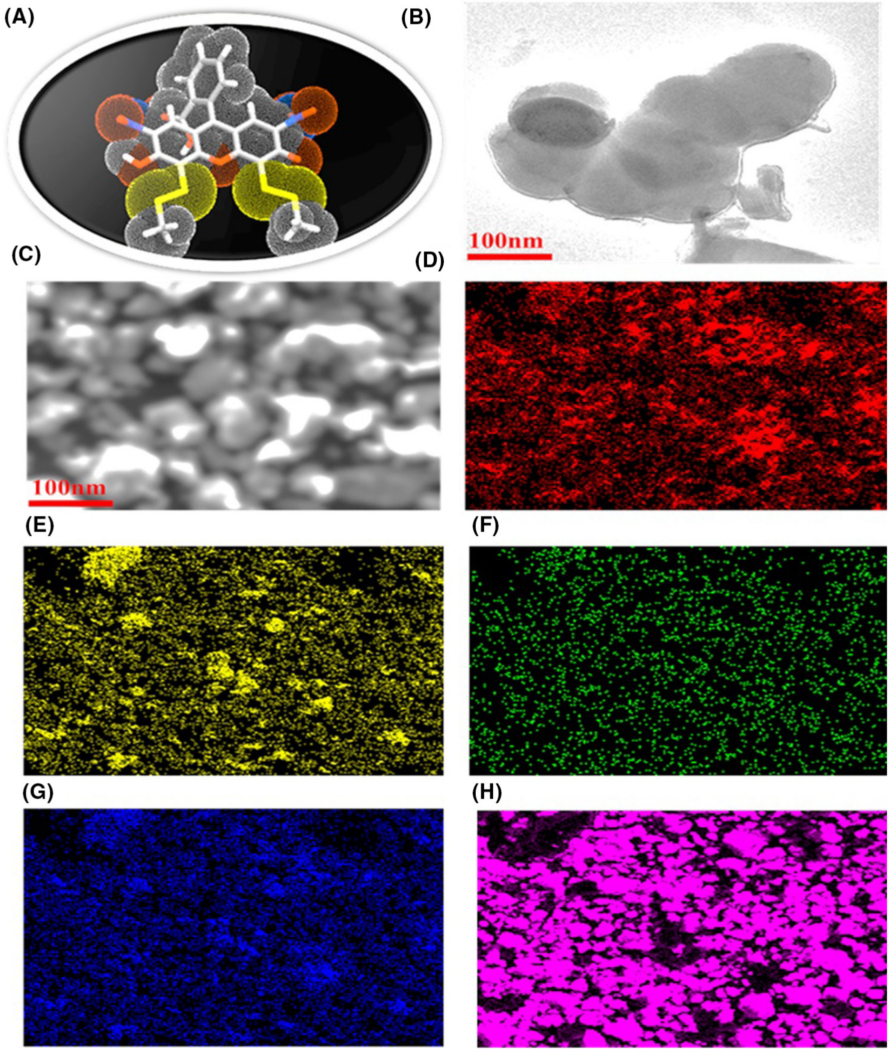

FIGURE 2 (A) 3D structure of the SDE-B photocatalyst. TEM image of (B) SDE-B, and (C) SEM image of SDE-B along with elemental mapping images of (D) carbon C (E) sodium (F) nitrogen, (G) oxygen, (H) sulfur.

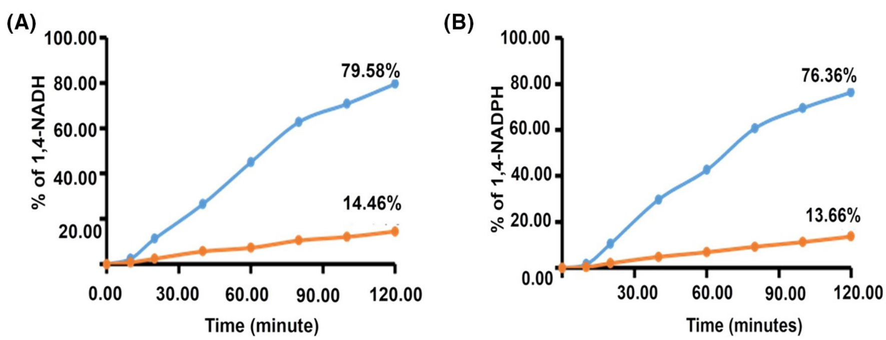

FIGURE 3 E-B and SDE-B photocatalyst's photocatalytic activity in 3.1 mL of neutral sodium phosphate buffer (100 mM) containing beta-NAD$^+$/NADP$^+$ (1.24 µmol), AsA (0.1 mmol), Rh (0.62 µmol), and SDE-B photocatalyst (5 mg).

by the term "dumbbell cloth-like flexible agglomerated structure". Dumbbell: Given that a dumbbell is normally made up of two spherical objects, this word implies that the observed structure may have a shape similar to a dumbbell, which typically consists of two spherical or ellipsoidal regions connected by a thinner bridge-like structure in the middle. Cloth-like: This adjective suggests that the structure may resemble a fabric or textile, perhaps with a web of intertwined fibers or strands. This can point to a complicated and well-planned arrangement of the material. Flexible: The adjective "flexible" implies that the constituent parts of this structure's material are not inflexible but rather capable of deforming or changing shape. Its special qualities may be connected to this adaptability. Agglomerated: The term "agglomerated" denotes a structure made up of a collection of separate elements or particles. These particles might be nanoparticles or other minute components that have come together to form a more substantial, cohesive assembly. The statement ends by saying that the excellent photocatalytic activity is confirmed by the observed structure. This suggests that the material's ability to efficiently catalyze photochemical processes, which is a desired attribute in different applications, such as environmental clean-up or energy conversion, is connected to the unique shape exhibited in Figure 2B. Overall, the information supplied provides an understanding of the physical structure of the material as revealed by TEM and its relationship to its photocatalytic activity, indicating that the observed morphology is extremely important to the material's functionality.

Poof of NADH/NADPH regeneration via cyclic voltammetry

Cyclic voltammetry, as seen in Figure 1D, offers an insightful look at the process's mechanics. NAD^+, ROC, and SDE-B were shown to have reduction potentials of around −0.51 eV, −0.71 V, and −1.01 V (Figure S2). A most important increase in the fixation peak current along with NAD^+ was also seen in the SDE-B-ROC, signifying that the system collected of SDE-B and ROC was able to catalyze the fixation of NAD^+ (Figure 1D). According to a recent publication, the catalytic impact of ROC causes a significantly higher rate of ROC decrease when NAD^+ is present.[40] Further evidence that SDE-B-ROC followed the electrochemistry of ROC came from the absence of an oxidation peak. The catalytic activity of the SDE-B-ROC complex may be attributed to the photoelectric behavior of SDE-B since the excited electron of SDE-B could be forwarded to ROC with ease. Researchers claim that the highest occupied molecular orbital (HOMO) excitation of the lowest occupied molecular orbital (LUMO), followed by the excited electrons transfer into the rhodium ROC, is the source of the hybrid light-harvesting molecule's photoelectrical property. In this instance, the electron photoexcites from HOMO (E = −5.48 eV) to LUMO (E = −3.64 eV) and then cascades into ROC (E = −3.96 eV) without emitting radiation. This effective electron transfer from the light-harvesting SDE-B photocatalyst to the electro-catalytic ROC center is made possible by the proximity and potential gradient between them. After being chemically protonated in aqueous environments, the resulting electrically reduced ROC, [Cp*Rh(bpy)], undergoes a catalytic interaction with $NAD^+/NADP^+$ that results in the regeneration of NADH/NADPH (79.58/76.36%).[68]

To investigate E-B and SDE-B photocatalyst for solar light-driven photo-regeneration of NADH/NADPH, photocatalytic experiments were conducted. The starting material E-B's capacity for photocatalytic NADH/NADPH regeneration was also investigated for the comparison sake. In both instances, the amount of photo-regenerated NADH/NADPH was quantified using UV–visible spectroscopy. As can be seen in Figure 3, SDE-B had notable effectiveness in NADH/NADPH photo-regeneration, accumulating NADH/NADPH at a steady rate up to 79.58/76.36% with time linearity. In totality, the newly designed photocatalyst is superior than E-B photocatalyst (Figure 3) due to high solar light-harvesting capacity and slow recombination charges. Therefore, the newly designed photocatalyst has additional significant application for organic transformation or oxygenation reaction (Table 1 and Figure 4).[69,70]

Furthermore, Figure S5 depicts the potential energy diagram associated with the generation and transmission of charge through artificial photosynthesis. Primarily, the generation of excited electron–hole pairs within the valence band (V.B.) of SDE-B photocatalyst [with a HOMO energy level of −5.48 eV] is triggered by the illumination of light, and this process is further facilitated by ascorbic acid, which moves the excited electrons into the conduction band (C.B.). Simultaneously, the excited electrons from SDE-B transition to NAD^+ from the C.B. [with a LUMO energy level of −3.64 eV] through the Rh-complex, which acts as an electron mediator, playing a role in the regeneration of NADH. This is attributed to the fact that the LUMO level (−3.64 eV) of

TABLE 1 Optimization of the oxygenation reaction conditions.

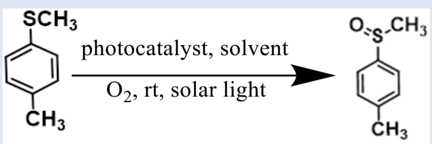

1a 1b

Entry	Photocatalyst	Solvent	Yield (%)
1.	SDE-B	DMSO	7
2.	SDE-B	DMF	21
3.	SDE-B	CH_3CN	36
4.	SDE-B	C_2H_5OH	25
5.	SDE-B	IPA	99.5
6.	E-B	IPA	35
7.	Without catalyst	IPA	Trace
8.	SDE-B without light	IPA	10

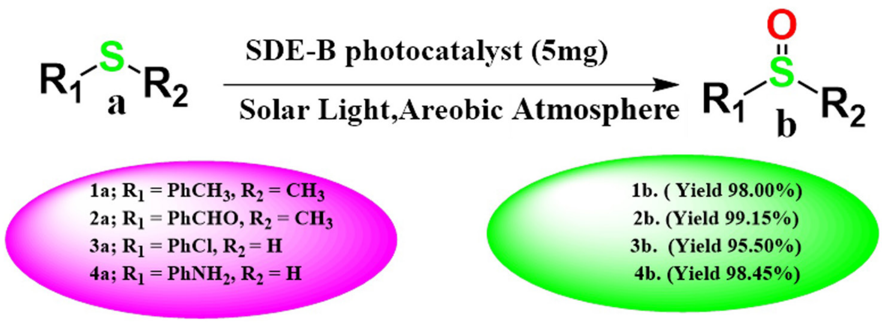

FIGURE 4 SDE-B photo-catalyzed selective oxygenation of sulfides.

SDE-B is higher than the potential levels of the Rh-complex (−3.96 eV) and NAD^+ (−4.20 eV). Consequently, excited electrons from SDE-B are seamlessly transferred to NAD^+, resulting in a more efficient regeneration of NADH.[71–73]

The electrochemical impedance spectra (EIS) were scrutinized to assess the behavior of charge carriers' separation/migration and current in a three-electrode system. The analysis was performed over a frequency spectrum spanning from 100 kHz down to 0.1 Hz, employing an AC amplitude of 5 mV. The separation distance between the working and reference electrodes was maintained at a constant 1 cm for all electrochemical assessments. In the figure, we have illustrated the Nyquist plot for both E-B and sulfur-doped eosin-B (SDE-B) photocatalysts. Both samples' Nyquist plots display a flattened and smaller semicircular shape. In line with the results reported in the cited articles,[74–76] the Nyquist plot for SDE-B reveals a reduced radius, signifying a notably improved capacity for the migration and transfer of photo-generated carriers. The structure of SDE-B provides a clear pathway for photo-induced electrons and holes to migrate to the surface, resulting in a further decrease in charge transfer resistance (Rct) for SDE-B. Furthermore, this reduced charge resistance indicates effective electron transfer and current increase during the proton reduction process at the interface between the photocatalyst and electrolyte, primarily attributed to the sulfur doping of E-B. Also, we checked the stability of the photocatalyst in Figure S7.

Oxygenation reaction via newly designed SDE-B photocatalyst under solar light

We started our research by investigating the oxidation of sulfides (1a) using 5 mg of SDE-B for 9 h under solar light from a blue LED (5 W) at room temperature (Table 1). The reaction was originally carried out in DMSO, but only a very small amount of the desired product was produced (Entry 1). The findings of the solvent optimization showed that solvents are crucial to the oxidation reactions (Entries 2–5). Low yields of products were produced using solvents such as DMF, CH_3CN, and C_2H_5OH (Entries 2–4), while IPA produced the maximum conversion (99.5%) after 9 h at room temperature (Entry 5), likely as a result of its higher surface area and polarizability than E-B (Entry 6). As a result, we (Entry 5) obtained the best yield (99.5%) and selectivity (100%). No excessive oxidation was seen. A trace amount of product (Entry 7) was produced when SDE-B was not used as the photocatalyst in this reaction because of its incredibly weak UV–Vis absorption in IPA. In this reaction, the SDE-B photocatalyst without light was also investigated, and less product was produced (Entry 8) because of the excitation of the electron. No reaction occurred in the absence of SDE-B (Entry 7) or light (Entry 8), according to the control trials.[69,77]

SDE-B photo-catalyzed selective oxygenation of sulfides

Reaction conditions

Sulfides (0.2 mmol), SDE-B photocatalyst (5 mg), and IPA (4.0 mL) equipped with an oxygen balloon under solar light at room temperature.

We explored the substrate scope of this technique after establishing optimal reaction conditions, utilizing 5 mg of SDE-B as a photocatalyst in an aerobic environment at ambient temperature and photo-irradiation with a blue LED (1.0 mW cm^{-2}) (Figure 4). The results show that distinct thioethers (1a-4a) had nearly equally acceptable yields and selectivity. All substituted derivatives of thioanisoles having electron donating or withdrawing functional groups at the aryl moiety (2a) were oxidized, although longer reaction durations were required to achieve high conversions (2b). Furthermore, the CH_3, Cl, and NH_2 groups were well-endured in this reaction (1a, 2a, and 4a), allowing for further functionalization. The rate of sulfoxidation was typically quicker in the aldehyde group containing thioethers (2a). Under these circumstances, the aldehyde group containing sulfides was oxidized to sulfoxides with excellent yields. Sulfide-containing CH_3, Cl, and NH_2 groups reacted slowly,

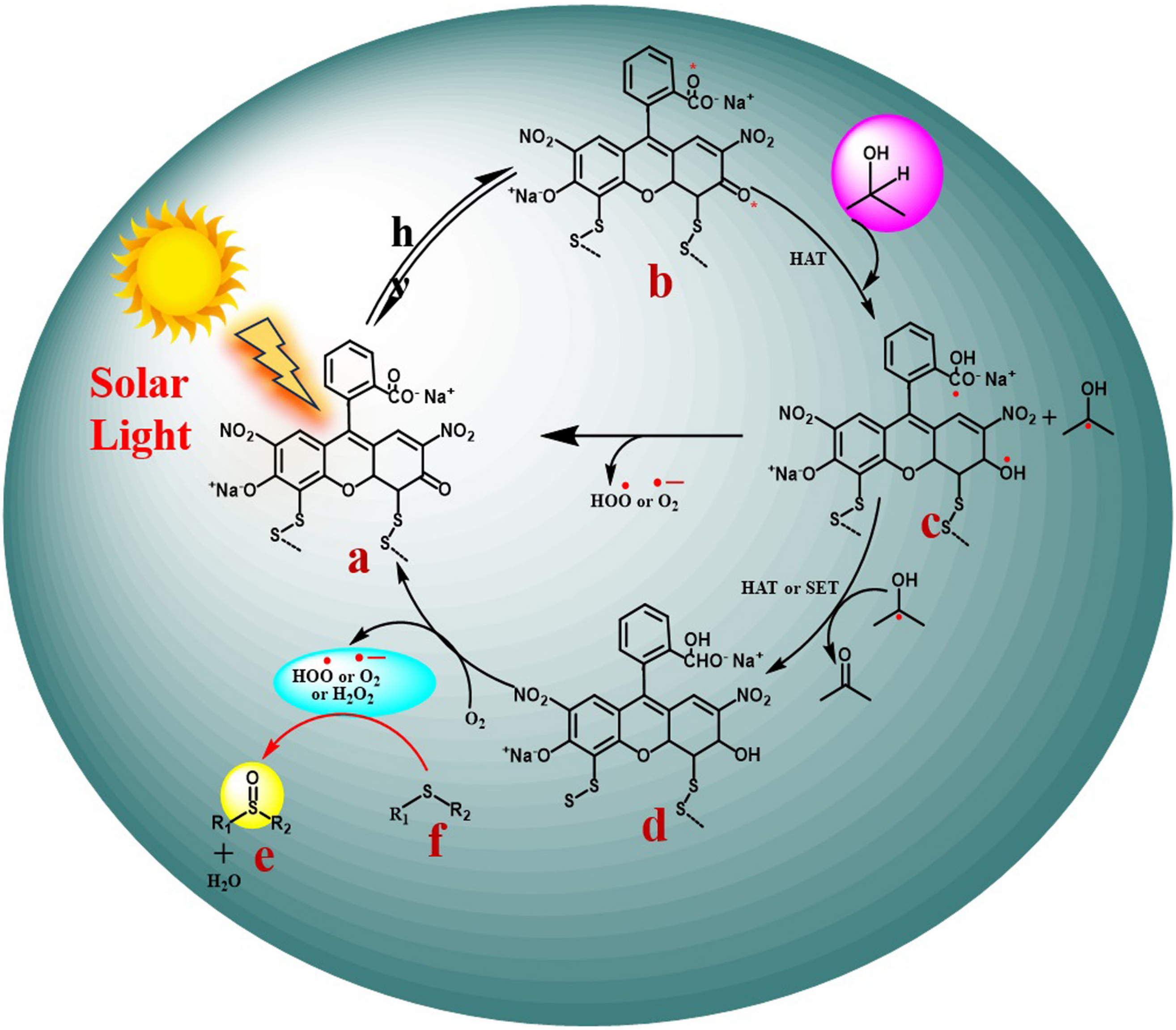

SCHEME 4 Proposed photocatalytic oxygenation of sulfides into sulfoxides reaction from newly designed SDE-B photocatalyst under solar light in aerobic condition.

presumably because to the less electron density on the sulfur atom.

Photocatalytic mechanistic investigations of oxygenation reactions

Photocatalytic mechanistic investigation of oxygenation reaction is shown in Schemes 1 and 4. In terms of mechanistic study, the process began with the activation by solar light of the SDE-B photocatalyst "a," which was subsequently transformed into "b." After accepting hydrogen atoms from IPA, the excited form "b" transforms into "c." Further accepting hydrogen atoms from IPA, the intermediate "c" transforms into "d" and produces acetone. The hydrogen acceptor was molecular oxygen, which changed into H_2O_2 after accepting a hydrogen atom from the intermediate "d." Along with the removal of the H_2O molecule, the generated H_2O_2 oxidizes the sulfides ("e") into their respective sulfoxides ("f"). In order to finish the photocatalytic cycle, the intermediate "d" was once more transformed into its initial state "a."[55]

CONCLUSION

In conclusion, the allure of natural photosynthesis motivates us. By using Eosin-B and sulfur-doped eosin-B (SDE-B) photocatalysts, we thus showed how to reduce and oxygenate NAD^+/$NADP^+$ and sulfides in an environmentally acceptable manner. The SDE-B photocatalyst's photocatalytic performance and important influencing elements for its practical application were scientifically investigated. In comparison with E-B, the SDE-B photocatalyst demonstrated better selective regeneration cofactor 1,4-NADH/NADPH and photocatalytic S=O bond formation, leading to a photocatalytic efficiency that was about sixfold higher under solar light medium. This study offers a simple method for developing an environmentally favorable benign photocatalyst with much higher photocatalytic activity for the production and regeneration of the S=O bond and 1,4-NADH/NADPH in the presence of solar light. Additionally, the SDE-B system may be capable of supporting the 1,4-NADH/NADPH-independent photocatalytic and photoenzymatic system for the widest range of applications.

ACKNOWLEDGMENTS

The authors would like to thank the Department of Chemistry and Environmental Science, MMMUT, Gorakhpur-273010, India, and Artificial Photosynthesis Research group, KRICT, Yuseong-gu, Daejeon, 34114, Republic of Korea for providing the infrastructure for pursuing Ph.D. works.

ORCID

Rajesh K. Yadav https://orcid.org/0000-0002-5320-5259
Satyam Singh https://orcid.org/0000-0001-8537-4594

REFERENCES

1. Yadav RK, Kumar A, Park NJ, Kong KJ, Baeg JO. A highly efficient covalent organic framework film photocatalyst for selective solar fuel production from CO_2. *J Mater Chem A*. 2016;4:9413-9418. doi:10.1039/c6ta01625a
2. Surur AS, Schulig L, Link A. Interconnection of sulfides and sulfoxides in medicinal chemistry. *Arch Pharm*. 2019;352:1-11. doi:10.1002/ardp.201800248
3. Qi M-Y, Conte M, Anpo M, Tang Z-R, Xu Y-J. Cooperative coupling of oxidative organic synthesis and hydrogen production over semiconductor-based photocatalysts. *Chem Rev*. 2021;121:13051-13085.
4. Hill CK, Hartwig JF. Site-selective oxidation, amination and epimerization reactions of complex polyols enabled by transfer hydrogenation. *Nat Chem*. 2017;9:1213-1221. doi:10.1038/nchem.2835
5. Kulkarni AR, Zhao ZJ, Siahrostami S, Nørskov JK, Studt F. Cation-exchanged zeolites for the selective oxidation of methane to methanol. *Cat Sci Technol*. 2018;8:114-123. doi:10.1039/c7cy01229b
6. Lang X, Zhao J, Chen X. Visible-light-induced photoredox catalysis of dye-sensitized titanium dioxide: selective aerobic oxidation of organic sulfides. *Angew Chem Int Ed Engl*. 2016;55:4697-4700. doi:10.1002/anie.201600405
7. Yang S, Peng L, Huang P, et al. Nitrogen, phosphorus, and sulfur Co-doped hollow carbon shell as superior metal-free catalyst for selective oxidation of aromatic alkanes. *Angew Chem Int Ed Engl*. 2016;55:4016-4020. doi:10.1002/anie.201600455
8. Caron S, Dugger RW, Ruggeri SG, Ragan JA, Brown Ripin DH. Large-scale oxidations in the pharmaceutical industry. *Chem Rev*. 2006;106:2943-2989. doi:10.1021/cr040679f
9. Chen K, Eschenmoser A, Baran PS. Strain release in C-H bond activation? *Angew Chem Int Ed Engl*. 2009;48:9705-9708. doi:10.1002/anie.200904474
10. Litvinas ND, Brodsky BH, Du Bois J. C-H hydroxylation using a heterocyclic catalyst and aqueous H_2O_2. *Angew Chem Int Ed Engl*. 2009;48:4513-4516. doi:10.1002/anie.200901353
11. Huang X, Groves JT. Beyond ferryl-mediated hydroxylation: 40 years of the rebound mechanism and C–H activation. *J Biol Inorg Chem*. 2017;22:185-207. doi:10.1007/s00775-016-1414-3
12. Howell JM, Feng K, Clark JR, Trzepkowski LJ, White MC. Remote oxidation of aliphatic C-H bonds in nitrogen-containing molecules. *J Am Chem Soc*. 2015;137:14590-14593. doi:10.1021/jacs.5b10299
13. Rackl D, Kreitmeier P, Reiser O. Synthesis of a polyisobutylene-tagged fac-Ir(ppy)3 complex and its application as recyclable visible-light photocatalyst in a continuous flow process. *Green Chem*. 2015;18:214-219. doi:10.1039/c5gc01792k
14. Lima CGS, Lima TDM, Duarte M, Jurberg ID, Paixão MW. Organic synthesis enabled by light-irradiation of EDA complexes: theoretical background and synthetic applications. *ACS Catal*. 2016;6:1389-1407. doi:10.1021/acscatal.5b02386
15. Prier CK, Rankic DA, MacMillan DWC. Visible light photoredox catalysis with transition metal complexes: applications in organic synthesis. *Chem Rev*. 2013;113:5322-5363. doi:10.1021/cr300503r
16. Tucker JW, Stephenson CRJ. Shining light on photoredox catalysis: theory and synthetic applications. *J Org Chem*. 2012;77:1617-1622. doi:10.1021/jo202538x
17. Prier CK, Rankic DA, Macmillan DWC. Cr300503R.Pdf. 2012.
18. Marin ML, Santos-Juanes L, Arques A, Amat AM, Miranda MA. Organic photocatalysts for the oxidation of pollutants and model compounds. *Chem Rev*. 2012;112:1710-1750. doi:10.1021/cr2000543
19. Ravelli D, Fagnoni M, Albini A. Photoorganocatalysis. What for? *Chem Soc Rev*. 2013;42:97-113. doi:10.1039/c2cs35250h
20. Haria DP, König B. Synthetic applications of eosin Y in photoredox catalysis. *Chem Commun*. 2014;50:6688-6699. doi:10.1039/c4cc00751d
21. Fukuzumi S, Ohkubo K. Organic synthetic transformations using organic dyes as photoredox catalysts. *Org Biomol Chem*. 2014;12:6059-6071. doi:10.1039/c4ob00843j
22. Pitre SP, McTiernan CD, Scaiano JC. Understanding the kinetics and spectroscopy of photoredox catalysis and transition-metal-free alternatives. *Acc Chem Res*. 2016;49:1320-1330. doi:10.1021/acs.accounts.6b00012
23. Doherty GA, Kamenecka T, McCauley E, et al. N-aryl 2,6-dimethoxybiphenylalanine analogues as VLA-4 antagonists. *Bioorg Med Chem Lett*. 2002;12:729-731. doi:10.1016/S0960-894X(02)00009-4
24. Hartz RA, Arvanitis AG, Arnold C, et al. Synthesis and evaluation of 2-anilino-3-phenylsulfonyl-6-methylpyridines as corticotropin-releasing factor1 receptor ligands. *Bioorg Med Chem Lett*. 2006;16:934-937. doi:10.1016/j.bmcl.2005.10.097
25. Artico M, Silvestri R, Massa S, et al. 2-sulfonyl-4-chloroanilino moiety: a potent pharmacophore for the anti-human immunodeficiency virus type 1 activity of pyrrolyl aryl sulfones. *J Med Chem*. 1996;39:522-530. doi:10.1021/jm950568w

26. Artico M, Silvestri R, Pagnozzi E, et al. Structure-based design, synthesis, and biological evaluation of novel pyrrolyl aryl sulfones: HIV-1 non-nucleoside reverse transcriptase inhibitors active at nanomolar concentrations. *J Med Chem*. 2000;43(9):1886-1891.
27. Fernández I, Khiar N. Recent developments in the synthesis and utilization of chiral sulfoxides. *Chem Rev*. 2003;103:3651-3705. doi:10.1021/cr990372u
28. Yang YC, Baker JA, Ward JR. Decontamination of chemical warfare agents. *Chem Rev*. 1992;92:1729-1743. doi:10.1021/cr00016a003
29. Li J-Y, Li Y-H, Qi M-Y, Lin Q, Tang Z-R, Xu Y-J. Selective organic transformations over cadmium sulfide-based photocatalysts. *ACS Catal*. 2020;10:6262-6280.
30. Qi M-Y, Conte M, Tang Z-R, Xu Y-J. Engineering semiconductor quantum dots for selectivity switch on high-performance heterogeneous coupling photosynthesis. *ACS Nano*. 2022;16:17444-17453.
31. Yadav RK, Baeg J-O, Hwan Oh G, et al. A photocatalyst–enzyme coupled artificial photosynthesis system for solar energy in production of formic acid from CO_2. *J Am Chem Soc*. 2012;134:11455-11461. doi:10.1021/ja3009902
32. Bryliakov KP, Talsi EP. Transition metal catalyzed asymmetric oxidation of sulfides: from discovery to recent trends. *Curr Org Chem*. 2012;16:1215-1242. doi:10.2174/138527212800564268
33. Dad'ová J, Svobodová E, Sikorski M, König B, Cibulka R. Photooxidation of sulfides to sulfoxides mediated by tetra-O-Acetylriboflavin and visible light. *ChemCatChem*. 2012;4:620-623. doi:10.1002/cctc.201100372
34. Chemistry G, Anastas P, Agency EP. 녹색 화학 (Green Chemistry). *Encycl Toxicol*. 2007;12:810-812. doi:10.1016/b0-12-369400-0/00463-4
35. Bonesi SM, Fagnoni M, Monti S, Albini A. Photosensitized oxidation of phenyl and tert-butyl sulfides. *Photochem Photobiol Sci*. 2004;3:489-493. doi:10.1039/b316891c
36. Bonesi SM, Fagnoni M, Albini A. Hammett correlations in the photosensitized oxidation of 4-substituted thioanisoles. *J Org Chem*. 2004;69:928-935. doi:10.1021/jo035679e
37. Bonesi SM, Torriani R, Mella M, Albini A. The photooxygenation of benzyl, heteroarylmethyl, and allyl sulfides. *European J Org Chem*. 1999;7:1723-1728. doi:10.1002/(SICI)1099-0690(199907)1999:7<1723::AID-EJOC1723>3.0.CO;2-fR
38. Bonesi SM, Mella M, D'Alessandro N, Aloisi GG, Vanossi M, Albinit A. Photosensitized oxygenation of benzyl ethyl sulfide. *J Org Chem*. 1998;63:9946-9955. doi:10.1021/jo9817927
39. Memarian HR, Mohammadpoor-Baltork I, Bahrami K. Photoinduced electron transfer reactions of aryl benzyl sulfides promoted by 2,4,6-triphenylpyrilium tetrafluoroborate (TP+BF4-). *Bull Korean Chem Soc*. 2006;27:106-110. doi:10.5012/bkcs.2006.27.1.106
40. Baciocchi E, Del Giacco T, Elisei F, et al. Electron transfer and singlet oxygen mechanisms in the photooxygenation of dibutyl sulfide and thioanisole in MeCN sensitized by N-methylquinolinium tetrafluoborate and 9,10-dicyanoanthracene. The probable involvement of a thiadioxirane intermediate in El. *J Am Chem Soc*. 2003;125:16444-16454. doi:10.1021/ja037591o
41. Bonesi SM, Fagnoni M, Albini A. Photosensitized electron transfer oxidation of sulfides: a steady-state study. *European J Org Chem*. 2008;2008:2612-2620. doi:10.1002/ejoc.200800048
42. Baciocchi E, Crescenzi C, Lanzalunga O. Photoinduced electron transfer reactions of benzyl phenyl sulfides promoted by 9,10-dicyanoanthracene. *Tetrahedron*. 1997;53:4469-4478. doi:10.1016/S0040-4020(97)00119-1
43. Clennan EL, Zhou W, Chan J. Mechanistic organic chemistry in a microreactor. Zeolite-controlled photooxidations of organic sulfides. *J Org Chem*. 2002;67:9368-9378. doi:10.1021/jo0261808
44. Suzuki K, Jeong J, Yamaguchi K, Mizuno N. Photoredox catalysis for oxygenation/deoxygenation between sulfides and sulfoxides by visible-light-responsive polyoxometalates. *New J Chem*. 2016;40:1014-1021. doi:10.1039/c5nj01045d
45. Lang X, Ma W, Chen C, Ji H, Zhao J. Selective aerobic oxidation mediated by TiO_2 photocatalysis. *Acc Chem Res*. 2014;47:355-363. doi:10.1021/ar4001108
46. Johnson JA, Zhang X, Reeson TC, Chen YS, Zhang J. Facile control of the charge density and photocatalytic activity of an anionic indium porphyrin framework via in situ metalation. *J Am Chem Soc*. 2014;136:15881-15884. doi:10.1021/ja5092672
47. Liu S, Yang MQ, Tang ZR, Xu YJ. A nanotree-like CdS/ZnO nanocomposite with spatially branched hierarchical structure for photocatalytic fine-chemical synthesis. *Nanoscale*. 2014;6:7193-7198. doi:10.1039/c4nr01227e
48. Zhang P, Wang Y, Li H, Antonietti M. Metal-free oxidation of sulfides by carbon nitride with visible light illumination at room temperature. *Green Chem*. 2012;14:1904-1908. doi:10.1039/c2gc35148j
49. Casado-Sánchez A, Gómez-Ballesteros R, Tato F, et al. Pt(II) coordination complexes as visible light photocatalysts for the oxidation of sulfides using batch and flow processes. *Chem Commun*. 2016;52:9137-9140. doi:10.1039/c6cc02452a
50. Ghosh I, Ghosh T, Bardagi JI, König B. Reduction of aryl halides by consecutive visible light-induced electron transfer processes. *Science*. 2014;346:725-728. doi:10.1126/science.1258232
51. Zeng L, Liu T, He C, Shi D, Zhang F, Duan C. Organized aggregation makes insoluble perylene diimide efficient for the reduction of aryl halides via consecutive visible light-induced electron-transfer processes. *J Am Chem Soc*. 2016;138:3958-3961. doi:10.1021/jacs.5b12931
52. Zhang Y, Yang X, Tang H, Liang D, Wu J, Huang D. Pyrenediones as versatile photocatalysts for oxygenation reactions with: in situ generation of hydrogen peroxide under visible light. *Green Chem*. 2020;22:22-27. doi:10.1039/c9gc03152a
53. Singh C, Chaubey S, Singh P, et al. Self-assembled carbon nitride/cobalt (III) porphyrin photocatalyst for mimicking natural photosynthesis. *Diamond Relat Mater*. 2020;101:107648. doi:10.1016/j.diamond.2019.107648
54. Chaubey S, Yadav RK, Tripathi SK, Yadav BC, Singh SN, Kim TW. Covalent triazine framework as an efficient photocatalyst for regeneration of NAD(P)H and selective oxidation of organic sulfide. *Photochem Photobiol*. 2021;98:150-159. doi:10.1111/php.13504
55. Barber J, Andersson B. Revealing the blueprint of photosynthesis. *Nature*. 1994;370:31-34.
56. Balzani V, Credi A, Venturi M. Photochemical conversion of solar energy. *ChemSusChem*. 2008;1(1–2):26-58. doi:10.1002/cssc.200700087

57. Barber J. Photosynthetic energy conversion: natural and artificial. *Chem Soc Rev*. 2009;38:185-196. doi:10.1039/b802262n
58. Bastian EJ, Martin RB. Disulfide vibrational spectra in the sulfur-sulfur and carbon-sulfur stretching region. *J Phys Chem*. 1973;77:1129-1133. doi:10.1021/j100628a010
59. Jiang HQ, Endo H, Natori H, Nagai M, Kobayashi K. Fabrication and photoactivities of spherical-shaped $BiVO_4$ photocatalysts through solution combustion synthesis method. *J Eur Ceram Soc*. 2008;28:2955-2962. doi:10.1016/j.jeurceramsoc.2008.05.002
60. Wang CA, Zhang ZK, Yue T, et al. 'Bottom-up' embedding of the Jørgensen-Hayashi catalyst into a chiral porous polymer for highly efficient heterogeneous asymmetric organocatalysis. *Chemistry*. 2012;18:6718-6723. doi:10.1002/chem.201200753
61. Wang CA, Han YF, Li YW, Nie K, Cheng XL, Zhang JP. Bipyridyl palladium embedded porous organic polymer as highly efficient and reusable heterogeneous catalyst for Suzuki-Miyaura coupling reaction. *RSC Adv*. 2016;6:34866-34871. doi:10.1039/c6ra03331h
62. Wang CA, Li YW, Hou XM, Han YF, Nie K, Zhang JP. N-heterocyclic carbene-based microporous organic polymer supported palladium catalyst for carbon-carbon coupling reaction. *ChemistrySelect*. 2016;1:1371-1376. doi:10.1002/slct.201600174
63. Rigter SA, Quinn XL, Kumar RE, et al. Passivation properties and formation mechanism of amorphous halide perovskite thin films. *Adv Funct Mater*. 2021;31:2010330. doi:10.1002/adfm.202010330
64. Galeski A. Strength and toughness of crystalline polymer systems. *Prog Polym Sci*. 2003;28(12):1643-1699. doi:10.1016/j.progpolymsci.2003.09.003
65. Kang Y, Yang Y, Yin LC, Kang X, Liu G, Cheng HM. An amorphous carbon nitride photocatalyst with greatly extended visible-light-responsive range for photocatalytic hydrogen generation. *Adv Mater*. 2015;27:4572-4577. doi:10.1002/adma.201501939
66. Slater AG, Cooper AI. Function-led design of new porous materials. *Science*. 2015;348:aaa8075. doi:10.1126/science.aaa8075
67. Ben T, Ren H, Shengqian M, et al. Targeted synthesis of a porous aromatic framework with high stability and exceptionally high surface area. *Angew Chem Int Ed Engl*. 2009;48:9457-9460. doi:10.1002/anie.200904637
68. Tripathi A, Yadav RK, Singh S, et al. A donor-acceptor self-assembled graphitic carbon nitride based EB-T photocatalytic system for generation and regeneration of C (sp3) F bond and NADH under sunlight. *Diamond Relat Mater*. 2023;136:109998.
69. Singh P, Chaubey S, Singh C, et al. Polystyrene-based eosin-Y as a photocatalyst for solar light-mediated NADH/NADPH regeneration and organic transformations. *React Chem Eng*. 2023;8:1072-1082.
70. Kumar K, Yadav RK, Verma RK, et al. Unleashing the solar revolution: harnessing the power of an ultra-strong tensile strength PGTPP nanocomposite photocatalyst for artificial photosynthesis. *Cat Sci Technol*. 2023;13:5679-5688.
71. Singh S, Yadav K, Wu R, et al. Generation and regeneration of the C(sp3)–F bond and 1,4-NADH/NADPH via newly designed S-gC3N4@Fe2O3/LC photocatalysts under solar light. *Energy Fuel*. 2022;36:8402-8412. doi:10.1021/acs.energyfuels.1c03697
72. Yadav RK, Baeg J-O, Kumar A, Kong K, Oh GH, Park N-J. Graphene–BODIPY as a photocatalyst in the photocatalytic–biocatalytic coupled system for solar fuel production from CO 2. *J Mater Chem A*. 2014;2:5068-5076.
73. Singh S, Yadav R, Kim T, et al. Rational design of a graphitic carbon nitride catalytic–biocatalytic system as a photocatalytic platform for solar fine chemical production from CO 2. *React Chem Eng*. 2022;7:1566-1572.
74. Riyajuddin S, Tarik Aziz SK, Kumar S, Nessim GD, Ghosh K. 3D-graphene decorated with g-C3N4/Cu3P composite: a Noble metal-free bifunctional electrocatalyst for overall water splitting. *ChemCatChem*. 2020;12:1394-1402.
75. Saha S, Sarkar P. Differential pulse anodic stripping voltammetry for detection of As (III) by chitosan-Fe (OH) 3 modified glassy carbon electrode: a new approach towards speciation of arsenic. *Talanta*. 2016;158:235-245.
76. Han X, Yuan A, Yao C, Xi F, Liu J, Dong X. Synergistic effects of phosphorous/sulfur co-doping and morphological regulation for enhanced photocatalytic performance of graphitic carbon nitride nanosheets. *J Mater Sci*. 2019;54:1593-1605.
77. Srivastava S, Yadav RK, Pande PP, et al. Dye degradation and sulfur oxidation of methyl orange and thiophenol via newly designed nanocomposite GQDs/NiSe-NiO photocatalyst under homemade LED light. *Photochem Photobiol*. 2023;99:1097-1105.

SUPPORTING INFORMATION

Additional supporting information can be found online in the Supporting Information section at the end of this article.

How to cite this article: Shukla RK, Yadav RK, Gole VL, Singh S, Gupta NK, Baeg J-O. Photocatalytic fixation and oxygenation of NAD^+/ $NADP^+$ and sulfides using solar light: Exploring mechanistic investigations and their impact on synthetic applications. *Photochem Photobiol*. 2023;00:1-12. doi:10.1111/php.13890